Three-dimensional imaging and recognition of microorganisms using computational holography

Bahram Javidi*[a], Seokwon Yeom[a], Inkyu Moon[a], and Edward Carapezza[b]

[a]Dept. of Electrical and Computer Engineering, U-2157, University of Connecticut, Storrs, CT USA 06269-2157;
[b]Defense Advanced Research Projects Agency (DARPA), 3701 N. Fairfax Drive, Arlington, VA USA 22203-1714

ABSTRACT

In this keynote address, we introduce three-dimensional (3D) sensing, visualization and recognition of microorganisms using microscopy-based single-exposure on-line (SEOL) digital holography. A coherent Mach-Zehnder interferometer records Fresnel diffraction field by a single on-line exposure to generate a microscopic digital hologram. Complex amplitude distribution is numerically reconstructed by the inverse Fresnel transform at arbitrary depth planes. After the reconstruction of volumetric complex images, 3D biological micro-objects are segmented and features are extracted by Gabor-based wavelets. The graph matching technique searches predefined 3D morphological shapes of reference biological microorganisms. Preliminary experimental results using sphacelaria alga and tribonema aequale alga are presented.

Keywords: Three-dimensional image processing; Holographic interferometry; Fourier optics; Feature extraction; Pattern recognition.

1. INTRODUCTION

Optical sensing and imaging have proven to be very useful in the design of two-dimensional (2D) and three-dimensional (3D) automatic target recognition (ATR) [1-14]. Growing interest in object recognition by means of 3D optical information system reflects its vast potential to achieve more reliable and robust system [4,8]. For example, we can sense and reconstruct 3D information by digital holography [15-21]. Non-linear filtering, neural networks, and statistical pattern recognition techniques are applied to digital holography for the purpose of object detection and identification [4-8]. Recently, real-time sensing, visualization, and recognition of biological microorganisms using digital holography are addressed in [8-11].

The applications of real-time imaging and recognition of microorganisms are very broad including biological weapon detection, medical and health care, and ecological monitoring. However, the reliable recognition of tiny and living organisms is very challenging. The small biological objects vary in size and shape among the same species, and they can move, grow, and reproduce themselves depending on environmental factors [22]. They may occur as a single cell or form an association of arbitrary complexity. Previously, various researches have been performed to recognize specific shapes of microorganisms based on 2D intensity images [23-28].

In this keynote address, we review 3D imaging and recognition of two filamentous microorganisms (sphacelaria alga and tribonema aequale alga) with computational holography [8,9]. Assuming that the microorganisms are individually segmented or they are sparsely aggregated, we identify two different microbiological objects with their morphological traits. Our system is composed of several stages as shown in Fig. 1. At the first stage, single-exposure on-line (SEOL) digital holography senses and visualizes the complex amplitude of microorganisms. Coherent microscopy-based Mach-Zehnder interferometer records the distribution of the complex wave generated by the Fresnel diffraction at a single hologram plane. The 3D information can be reconstructed from the digital hologram at an arbitrary depth plane by means of the inverse Fresnel transform. For automated 3D recognition, reconstructed images are processed by segmentation, feature extraction, and graph matching technique. For preprocessing, reconstructed images are resized and objects of interest are segmented from the background diffraction fields. We segment foreground objects using histogram analysis and maximum intensity transmitted [8-11]. Gabor-based wavelets extract salient features by decomposing segmented

*bahram@engr.uconn.edu; phone 1 860 486-2867; fax 1 860 486-6339

Automatic Target Recognition XVI, edited by Firooz A. Sadjadi, Proc. of SPIE Vol. 6234, 623405, (2006) · 0277-786X/06/$15 · doi: 10.1117/12.664209

images in the spatial frequency domain [29,30]. Rigid graph matching (RGM) with Gabor-features realizes template matching between a reference and an unknown input microorganism sample. During the RGM, we assume that a reference graph is predetermined in order to represent the unique shape feature of the reference microorganism in our database and we search similar shapes with that of the reference microorganism. The RGM combined with Gabor-based wavelets has proven to be a robust template matching technique which is invariant to shift, rotation, and distortion [12,13].

In Section 2, we present an overview of SEOL digital holography and its advantages. Feature extraction using Gabor-based wavelets is described in Sections 3. The graph matching technique is illustrated in Section 4. In Section 5, experimental results are presented. Conclusions follow in Section 6.

2. SINGLE EXPOSURE ON-LINE (SEOL) DIGITAL HOLOGRAPHY

In the following, we review the principles and advantages of SEOL digital holography. SEOL digital holography has several advantages beyond off-axis digital holography and phase-shifting on-line digital holography [6-9]. First, in SEOL digital holography, real-time processing is possible since it requires only one single-exposure. Second, we can achieve a more reliable system which is robust to environmental fluctuation and noise. Thus, it is suitable to detect dynamic scenes of micro-biological events. The schematic setup of the SEOL digital holography recording is illustrated in Fig. 2. Polarized light from an Argon laser with a center wavelength (λ) of 514.5 nm, is expanded by a spatial filter and a collimating lens to provide spatial coherence. The expanded beam is divided into object and reference beam by a beam splitter. The object beam illuminates the microorganism sample and the microscope objective produces a magnified image positioned at the image plane of the microscope. The reference beam forms an on-line interference pattern together with the light diffracted by the microorganism sample and the interference pattern is recorded by the CCD array. Since SEOL digital holography needs only one single-exposure, our system uses no optical components for the phase retardation in the reference beam which phase-shifting digital holography requires.

In the following, we describe both on-axis phase-shifting digital holography and SEOL digital holography. In the experiments, both of phase-shifting on-axis digital holography with double exposure and SEOL digital holography are implemented to obtain experimental results for the visualization of 3D biological objects. The results of SEOL digital holography are compared with those of multiple-expose phase-shifting digital holography.

We start our discussion by describing on-axis phase-shifting digital holography [20]. The hologram recorded on the CCD array can be represented as follows:

$$H_p(x,y) = [A_H(x,y)]^2 + A_R^2 + 2A_H(x,y)A_R \times \cos[\Phi_H(x,y) - \varphi_R - \Delta\varphi_p], \quad (1)$$

where $A_H(x,y)$ and $\Phi_H(x,y)$ are the amplitude and phase, respectively, of the Fresnel complex field of the micro objects at the recording plane generated by the object beam, A_R is the amplitude of the reference distribution, φ_R denotes the constant phase of the reference beam, and $\Delta\varphi_p$, where the subscript p is an integer from 1 and 4, denotes the four possible phase shifts required for on-axis phase-shifting digital holography. The desired Fresnel wave function of the biological object, $A_H(x,y)$ and $\Phi_H(x,y)$ can be obtained by use of the four interference patterns with different phase shifts, $\Delta\varphi_p = 0$, $\pi/2$, π, and $3\pi/2$. Therefore, the double-exposure method requires: 1) two interference patterns that have a $\pi/2$ phase difference, 2) the information about a reference beam, and 3) information about the intensity of diffracted object beam. The complex amplitude at the hologram plane from the double-exposure method is represented by:

$$\begin{aligned} U_h(x,y) &= A_H(x,y) \times \cos[\Phi_H(x,y)] + jA_H(x,y) \times \sin[\Phi_H(x,y)] \\ &= \{H_1(x,y) - A_H(x,y)^2 - A_R{}^2\}/(2A_R) + j\{H_2(x,y) - A_H(x,y)^2 - A_R{}^2\}/(-2A_R), \end{aligned} \quad (2)$$

where $H_1(x,y)$ and $H_2(x,y)$ can be obtained from Eq. (1). We assume that the recording between two holograms is uniform and reference beam is plane wave. It is noted that the former assumption requires stable recording environment and stationary objects. However, SEOL digital holography needs only one single-exposure to sense the complex amplitude of 3D biological objects, therefore, it is suitable for recording fast dynamic events and more robust to fluctuation and noise [6]. The information about the wave front of a 3D biological object contained in the SEOL digital hologram is represented as:

$$U_{h'}(x,y) = 2A_H(x,y)A_R \times \cos(\Phi_H(x,y) - \varphi_R) = H_1(x,y) - |A_H(x,y)|^2 - A_R^2 . \quad (3)$$

In Eq. (3), $H_1(x,y)$ can be obtained from Eq. (1). To remove DC terms in Eq. (3), the reference beam intensity $|A_R|^2$ is recorded by only one time measuring in the experiment. The object beam intensity $|A_H(x,y)|^2$ can be considerably reduced by use of signal processing (for example, averaging technique). Thus, the 3D biological object wave function $U_{h'}(x,y)$ including a conjugate component in Eq. (3) can be obtained by use of SEOL digital holography. In this keynote address, we show that $U_{h'}(x,y)$ in Eq. (3) obtained by a SEOL hologram can be used for 3D image formation and 3D biological object recognition. The imaging results will be compared with that of $U_h(x,y)$ in Eq. (2) obtained by on-line phase-shifting holography which requires multiple recordings. The microscopic 3D biological object can be restored by the Fresnel propagation of $U_{h'}(x,y)$ which is the biological object wave information in the hologram plane. We can numerically reconstruct 3D sectional images on any parallel planes perpendicular to the optical axis by computing the following inverse Fresnel transform:

$$U_{o'}(m',n') = \exp[-j\frac{\pi}{\lambda d}(\Delta X^2 m'^2 + \Delta Y^2 n'^2)] \times$$

$$\sum_{m=1}^{N_x}\sum_{n=1}^{N_y} U_{h'}(m,n)\exp[-j\frac{\pi}{\lambda d}(\Delta x^2 m^2 + \Delta y^2 n^2)]\exp[j2\pi(\frac{mm'}{N_x} + \frac{nn'}{N_y})], \quad (4)$$

where $U_{o'}(m',n')$ and $(\Delta X, \Delta Y)$ are the reconstructed complex amplitude distribution and resolution at the reconstruction plane, respectively, $U_{h'}(m,n)$ and $(\Delta x, \Delta y)$ are the object wave function including a conjugate component and resolution at the hologram plane, respectively, d represents the distance between the reconstruction plane and hologram plane, and N_x and N_y are the size of the hologram in the x and y directions.

3. FEATURE EXTRACTION USING GABOR-BASED WAVELETS

In this section, we provide a review of Gabor-based wavelets and feature extraction. Gabor-based wavelets are composed of multi-oriented and multi-scaled Gaussian-form kernels (impulse responses). The Gaussian-envelope in Gabor-based wavelets achieves the minimum space-bandwidth product [29]. Therefore, it is suitable to extract local features with high frequency bandwidth kernels and global features with low frequency bandwidth kernels. The impulse response of Gabor-based wavelets is the Gaussian envelope modulated by the complex sinusoidal function [30]:

$$g(\mathbf{x}) = \frac{|\mathbf{k}|^2}{\sigma^2}\exp\left(-\frac{|\mathbf{k}|^2|\mathbf{x}|^2}{2\sigma^2}\right)\left[\exp(j\mathbf{k}\cdot\mathbf{x}) - \exp\left(-\frac{\sigma^2}{2}\right)\right], \quad (5)$$

where $\mathbf{x}$ is a position vector, $\mathbf{k}$ is a wave number vector, and σ is proportional to the standard deviation of the Gaussian envelope. By changing the magnitude and direction of the vector $\mathbf{k}$, we can scale and rotate the Gabor kernel to make self-similar forms. We can define a discrete version of the Gabor kernel as $g_{uv}(m,n)$ at $\mathbf{k} = \mathbf{k}_{uv}$ and $\mathbf{x} = [m\ n]^t$, where m and n are discrete coordinates in the x and y directions, respectively, and the superscript t denotes transpose. Sampling of $\mathbf{k}$ is done as $\mathbf{k}_{uv} = k_{0u}[\cos\phi_v\ \sin\phi_v]^t$, $k_{0u} = k_0/\delta^{u-1}$, $\phi_v = [(v-1)/V]\pi$, $u = 1,\ldots,U$, and $v = 1,\ldots,V$, where k_{0u} is the magnitude of the wave number vector, ϕ_v is the azimuth angle of the wave number vector, k_0 is the maximum carrier frequency of the Gabor kernels, δ is the spacing factor in the frequency domain, and U and V are the total numbers of decompositions along the radial and tangential axes, respectively.

Let $h_{uv}(m,n)$ be the filtered output of the image $o(m,n)$ after it is convolved with the Gabor kernel $g_{uv}(m,n)$:

$$h_{uv}(m,n) = \sum_{m'=1}^{N_m}\sum_{n'=1}^{N_n} g_{uv}(m-m', n-n')o(m',n'), \quad (6)$$

where $o(m,n)$ is the normalized image between 0 and 1 after the segmentation, and N_m and N_n are the size of reconstructed images in the x and y directions, respectively. $h_{uv}(m,n)$ is also called the "Gabor coefficient."

We define a rotation-invariant node vector at a pixel with a set of the Gabor coefficients and the segmented image. The rotation-invariant property can be achieved by adding up all the Gabor coefficients along the tangential axes in the frequency domain. The rotation-invariant vector $\mathbf{v}$ is defined as:

$$\mathbf{v}(m,n) = \left[o(m,n) \sum_{v=1}^{V} h_{1v}(m,n) \cdots \sum_{v=1}^{V} h_{Uv}(m,n) \right]^t . \tag{7}$$

In the experiments, we use only real parts of the node vector since they are more suitable to represent filamentous structures. There is no optimal way to choose the parameters for the Gabor kernels, but several values are widely used heuristically depending on the applications [29,30]. The parameters are set up at $\sigma = \pi$, $k_0 = \pi/4$, $\delta = \sqrt{2}$, $U = 3$, and $V = 6$ in the experiments.

4. RIGID GRAPH MATCHING

In this section, we describe the graph matching technique. A template matching is performed between two graphs representing the morphological feature of microorganisms. The graph is defined as a set of adjacent nodes in the local area. Let R and S be two identical and rigid graphs placed on the reference image (o_r) and the unknown input image (o_s), respectively. The location of the reference graph R is pre-determined by the translation vector $\mathbf{p}_r$ and the clockwise rotation angle θ_r. A position vector of the node k in the graph R is computed as:

$$\mathbf{x}_k(\mathbf{p}_r, \theta_r) = \mathbf{A}(\theta_r)\left(\mathbf{x}_k^o - \mathbf{x}_c^o\right) + \mathbf{p}_r, \quad k = 1,\ldots,K, \tag{8}$$

$$A(\theta) = \begin{bmatrix} \cos\theta & \sin\theta \\ -\sin\theta & \cos\theta \end{bmatrix}, \tag{9}$$

where $\mathbf{x}_k^o$ and $\mathbf{x}_c^o$ are, respectively, the position of the node k and the center of the graph which is located at the origin without rotation, K is the total number of nodes in the graph, and A is a rotation matrix. Assuming the graph R covers a designated shape of the reference microorganism, we search the similar local morphology by translating and rotating the graph S on unknown input images. We describe any rigid motion of the graph S as follows:

$$\mathbf{x}_k(\mathbf{p}_s, \theta_s) = \mathbf{A}(\theta_s)\left(\mathbf{x}_k^o - \mathbf{x}_c^o\right) + \mathbf{p}_s, \quad k = 1,\ldots,K, \tag{10}$$

where $\mathbf{x}_k(\mathbf{p}_s, \theta_s)$ is a position vector of the node k of the graphs S after translated by $\mathbf{p}_s$ and rotated by θ_s. Two metrics are considered to decide identification between two graphs. One is a similarity function between the graph R and S which is defined as:

$$\Gamma_{rs} = \frac{1}{K} \sum_{k=1}^{K} \frac{\left\langle \mathbf{v}_r[\mathbf{x}_k(\mathbf{p}_r, \theta_r)], \mathbf{v}_s[\mathbf{x}_k(\mathbf{p}_s, \theta_s)] \right\rangle}{\| \mathbf{v}_r[\mathbf{x}_k(\mathbf{p}_r, \theta_r)] \| \| \mathbf{v}_s[\mathbf{x}_k(\mathbf{p}_s, \theta_s)] \|}, \tag{11}$$

where $\langle \cdot \rangle$ stands for the inner product of two vectors, and $\mathbf{v}_r[\mathbf{x}_k(\mathbf{p}_r, \theta_r)]$ and $\mathbf{v}_s[\mathbf{x}_k(\mathbf{p}_s, \theta_s)]$ are node vectors defined in Eq. (7) of the graph R and S respectively. Another metric is a difference cost function which is defined as:

$$C_{rs} = \frac{1}{K} \sum_{k=1}^{K} \left\| \mathbf{v}_r[\mathbf{x}_k(\mathbf{p}_r, \theta_r)] - \mathbf{v}_s[\mathbf{x}_k(\mathbf{p}_s, \theta_s)] \right\|. \tag{12}$$

To utilize the depth information of 3D reconstruction of the SEOL hologram, we simultaneously use multiple references which are reconstructed at different depths. The similarity function and the difference cost are measured by the node vectors between the graph R on the image o_{r_j} and the graph S on the image o_s. The graph R covers the fixed region in the reference images, "o_{r_j}", $j = 1,\ldots,J$ where J is the total number of reference images reconstructed at different depths. The graph S is identified with the reference shape which is covered by the graph R if two conditions are satisfied as follows:

$$\Gamma_{r_j s}(\mathbf{p}_s, \hat{\theta}_{s,\hat{j}}) > \alpha_\Gamma \text{ and } C_{r_j s}(\mathbf{p}_s, \hat{\theta}_{s,\hat{j}}) < \alpha_C, \tag{13}$$

$$\hat{j} = \max_j [\Gamma_{r_j s}(\mathbf{p}_s, \hat{\theta}_{s,j};)], \qquad \hat{\theta}_{s,j} = \arg\max_{\theta_s} [\Gamma_{r_j s}(\mathbf{p}_s, \theta_s)], \tag{14}$$

where α_Γ and α_C are thresholds for the similarity function and the difference cost, respectively, $\hat{j}$ is the index of the reference image which produces the maximum similarity between the graph R and the graph S with the translation

vector $\mathbf{p}_s$ and the rotation angle $\hat{\theta}_{s,j}$, and $\hat{\theta}_{s,j}$ is obtained by searching the best matching angle to maximize the similarity function.

5. EXPERIMENTAL RESULTS

In this section, we present experimental results of visualization and recognition of two filamentous microorganisms (sphacelaria alga and tribonema aequale alga). First, we sense and visualize microorganisms using SEOL holography, and compare the results with phase-shifting on-line digital holography. Second, automatic recognition is performed by processing reconstructed images with segmentation, feature extraction, and graph matching.

5.1 3D imaging with SEOL digital holography

In this subsection, we experimentally compare the 3D visualization of SEOL digital holography with that of multiple-exposure phase-shifting on-line digital holography. The images are reconstructed from digital holograms with 2048 × 2048 pixels and a pixel size of 9 μm × 9 μm. The microorganisms are sandwiched between two transparent cover slips. The diameter of the microorganisms is around 10~50 μm. We generate two holograms for the alga samples. The microscopic 3D biological object is placed at a distance 500 mm from the CCD array as shown in Fig. 2. The results of the reconstructed images from the hologram of the alga samples are shown in Fig. 3. Figure 3(a) and (b) shows sphacelaria's 2D image and the digital hologram by SEOL digital holography, respectively. Figure 3(c) and (d) are sphacelaria's reconstructed images from the blurred digital holograms at distance d = 180 mm and 190 mm, respectively using the SEOL digital holography. Figure 3(e) shows the sphacelaria's reconstructed image at distance d =180 mm using phase-shifting on-line digital holography with two interferograms, and Fig. 3(f) is tribonema aequale's reconstructed image at distance d =180 mm using SEOL digital holography. In the experiments, we use a weak reference beam for the conjugate image which overlaps the original image. As shown in Fig. 3, we obtain the sharpest reconstruction at distance that is between 180 mm and 190 mm for both holographic methods. The reconstruction results indicate that we obtain the focused image by use of SEOL digital holography as well as from the phase-shifting digital holography. We will show that SEOL digital holography may be a useful method for 3D biological object recognition. That is because the conjugate image in the hologram contains information about the 3D biological object. In addition, SEOL digital holography can be performed without stringent environmental stability conditions.

5.2 3D morphology-based recognition

To test the robustness of the system, we generate 8 hologram samples from sphacelaria and tribonema aequale, respectively. We denote 8 sphacelaria samples as $A_1,\ldots,A_8$ and 8 tribonema aequale samples as $B_1,\ldots,B_8$. Since we have changed the position of the CCD array during the experiments, the depths for the focused image are different. The samples A_1-A_3 are reconstructed at 180 mm, A_4-A_6 are reconstructed at 200 mm, and A_7 and A_8 are reconstructed at 300 mm, and all samples of tribonema aequale (B_1-B_8) are reconstructed at 180 mm for the sharpest images. Computationally reconstructed holographic images are cropped and reduced into images with 256×256 pixels by the reduction ratio 0.25. Segmentation is performed by the histogram analysis of reconstructed images [8-11]. During the segmentation we assume less than 25% of lower intensity region is occupied by the microorganisms and the intensity of the microorganisms is less than 45% of the background diffraction field.

To recognize two filamentous objects which have different thicknesses and distributions, a rectangular grid is selected as a reference graph for sphacelaria which shows regular thickness in the reconstructed images. The reference graph is composed of 25×3 nodes and the distance between nodes is 4 pixels in the x and y directions. Therefore, the total number of nodes in the graph is 75. The reference graph R is located in the sample A_1 with $\mathbf{p}_r = [81\ 75]^t$ and $\theta_r = 135°$ as shown in Fig. 4(a). To utilize the depth information, 4 reference images are used. They are reconstructed at distance d = 170, 180, 190, and 200 mm, respectively. The threshold α_Γ and α_C are set at 0.65 and 1, respectively. Thresholds are selected heuristically to produce better results. Considering the computational load, the graph S is translated by every 3 pixels in the x and y directions for measuring its similarity and difference with the graph R. To search the best matching angles, the graph S is rotated by 7.5° from 0 to 180° at every translated location. When the positions of rotated nodes are not integers, they are replaced with the nearest neighbor nodes. Figure 4(b) shows one sample (A_8) of test images with the RGM process. The reference shapes are detected 62 times along the filamentous objects. Figure 4(c) shows the number of detections for 16 samples. The detection number for A_1-A_8 varies from 31 to 251 showing strong

similarity between the reference image (A_1) and test images (A_2-A_8) of the same microorganism. There is no detection found in B_1-B_8. Figure 4(d) shows the maximum similarity and the minimum difference cost for all samples.

6. CONCLUSIONS

In this keynote address, we have overviewed 3D sensing, visualization and recognition technique using SEOL digital holography. Preliminary results are presented for real time and automatic recognition of microorganisms by examining their simple morphological traits. The principle and advantages of SEOL digital holography has been described. 3D imaging with SEOL digital holography is suitable for monitoring dynamic events of living micro-objects and more robust to noisy environments than multiple exposure phase-shifting digital holography. For the automatic recognition, segmentation, feature extraction by the Gabor-based wavelets, and graph matching technique are applied. The graph matching technique localizes specific shape features of the reference in unknown images. Preliminary results with two filamentous algae are presented for 3D imaging and recognition. The presented approach may have great benefits in medical treatments, environmental monitoring, and defense applications.

REFERENCES

1. A. Mahalanobis, R. R. Muise, S. R. Stanfill, and A. V. Nevel, "Design and application of quadratic correlation filters for target detection," IEEE Trans. on AES. 40, 837-850 (2004)
2. F. A. Sadjadi, "Infrared target detection with probability density functions of wavelet transform subbands," Appl. Opt. 43, 315-323 (2004).
3. H. Sjoberg, F. Goudail, and P. Refregier, "Optimal algorithms for target location in nonhomogeneous binary images," J. Opt. Soc. Am. A. 15, 2976-2985 (1998)
4. B. Javidi, ed., *Image Recognition and Classification: Algorithms, Systems, and Applications*, Marcel Dekker, New York, 2002.
5. B. Javidi and E. Tajahuerce, "Three dimensional object recognition using digital holography," Opt. Lett. 25, 610-612 (2000).
6. B. Javidi and D. Kim, "Three-dimensional-object recognition by use of single-exposure on-axis digital holography," Opt. Lett. 30, 236-238 (2005).
7. D. Kim and B. Javidi, "Distortion-tolerant 3-D object recognition by using single exposure on-axis digital holography," Opt. express 12, 5539-5548 (2005).
8. B .Javidi, ed., *Optical Imaging Sensors and Systems for Homeland Security Applications*, Springer, NewYork, 2006.
9. B. Javidi, I. Moon, S. Yeom, and E. Carapezza, "Three-dimensional imaging and recognition of microorganism using single-exposure on-line (SEOL) digital holography," Opt. Express 13, 4492-4506 (2005).
10. S. Yeom, I Moon, and B. Javidi, "Real-time 3D sensing, visualization and recognition of dynamic biological micro-organisms," Proceedings of IEEE 94, 550-566 (2006).
11. B. Javidi, I. Moon, and S. Yeom, "3D microorganism sensing, visualization and recognition using single exposure on-line digital holography," Optics and Photonics News 17, 16-21 (2006).
12. M. Lades, J. C. Vorbruggen, J. Buhmann, J. Lange, C. v.d. Malsburg, R. P. Wurtz, and W. Konen, "Distortion invariant object recognition in the dynamic link architecture," IEEE Trans. on Computers 42, 300-311 (1993).
13. S. Yeom, B. Javidi, Y. J. Roh, and H. S. Cho, "Three-dimensional object recognition using x-ray imaging," Opt. Eng. 43, (2005).
14. F. Sadjadi, "Improved target classification using optimum polarimetric SAR signatures," IEEE Trans. on AES. 38, 38-49 (2002).
15. O. Matoba, T. J. Naughton, Y. Frauel, N. Bertaux, and B. Javidi, "Real-time three-dimensional object reconstruction by use of a phase-encoded digital hologram," Appl. Opt. 41, 6187-6192 (2002).
16. B. Javidi and F. Okano, eds., *Three-dimensional Television, Video, and Display Technologies*, Springer, New York, 2002.
17. J. W. Goodman and R. W. Lawrence, "Digital image formation from electronically detected holograms," Appl. Phy. Lett. 11, 77-79 (1967).
18. T. M. Kreis and W. P. O. Juptner, "Suppression of the dc term in digital holography," Opt. Eng. 36, 2357-2360 (1997).
19. G. Pedrini and H. J. Tiziani, "Short-coherence digital microscopy by use of a lensless holographic imaging system," Appl. Opt. 41, 4489-4496 (2002).

20. T. Zhang and I. Yamaguchi, "Three-dimensional microscopy with phase-shifting digital holography," Opt. Lett. 23, 1221 (1998).
21. Alexander Stadelmaier and Jurgen H. Massig, "Compensation of lens aberrations in digital holography," Opt. Lett. 25, 1630 (2000).
22. J. W. Lengeler, G. Drews, and H. G. Schlegel, *Biology of the prokaryotes*, Blackwell science, New York, 1999.
23. M. G. Forero, F. Sroubek, and G. Cristobal, "Identification of tuberculosis bacteria based on shape and color," Real-time imaging 10, 251-262 (2004)
24. J. Alvarez-Borrego, R. R. Mourino-Perez, G. Cristobal-Perez, and J. L. Pech-Pacheco, "Invariant recognition of polychromatic images of Vibrio cholerae 01," Opt. Eng. 41, 872-833 (2002)
25. A. L. Amaral, M. da Motta, M. N. Pons, H. Vivier, N. Roche, M. Moda, and E. C. Ferreira, "Survey of protozoa and metazoa populations in wastewater treatment plants by image anlaysis and discriminant analysis," Environmentrics 15, 381-390 (2004)
26. S.-K. Treskatis, V. Orgeldinger, H. wolf, and E. D. Gilles, "Morphological characterization of filamentous microorganisms in submerged cultures by on-line digital image analysis and Pattern recognition," Biotechnology and bioengineering 53, 191-201 (1997).
27. T. Luo, K. Kramer, D. B. Goldgof, L. O. Hall, S. Samson, A. Remsen, and T. Hopkins, "Recognizing plankton images from the shadow image particle profiling evaluation recorder," IEEE Trans. on systems, man, and cybernetics Part B 34, 1753-1762 (2004).
28. J. M. S. Cabral, M. Mota, and J. Tramper eds., Multiphase bioreactor design: chap2 image analysis and multiphase bioreactor, (Taylor & Francis, London 2001)
29. J. G. Daugman, "Uncertainty relation for resolution in space, spatial frequency, and orientation optimized by two-dimensional visual cortical filters," J. Opt. Soc. Am. 2, 1160-1169 (1985).
30. T. S. Lee, "Image representation using 2D Gabor wavelets," IEEE Trans. on PAMI. 18, 959-971 (1996).

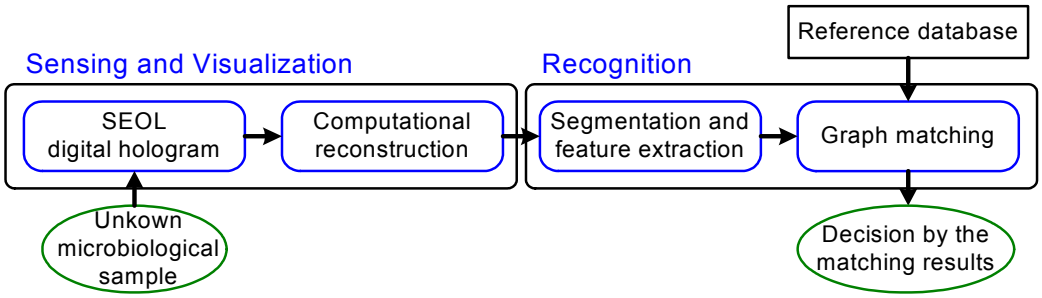

Fig. 1. Block diagram of the 3D visualization and recognition system.

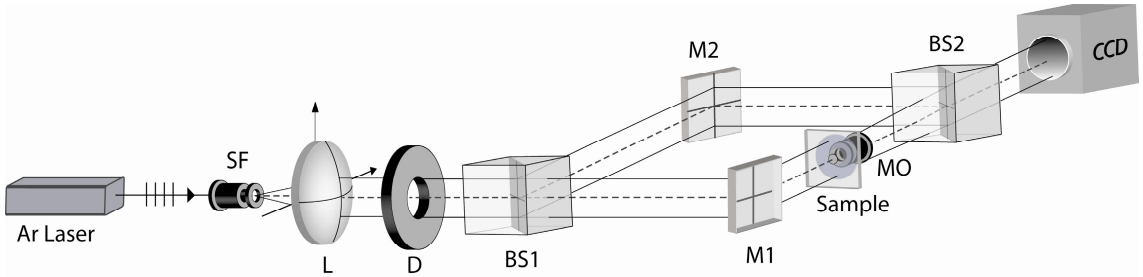

Fig. 2. Experimental setup for recording an on-line digital hologram of a microscopic 3D biological object; Ar: Argon laser, SF: spatial filter, L: lens, D: diaphragm, BS1, BS2: beam splitter; M1, M2: mirror; MO: microscope objective; CCD: charge coupled device array.

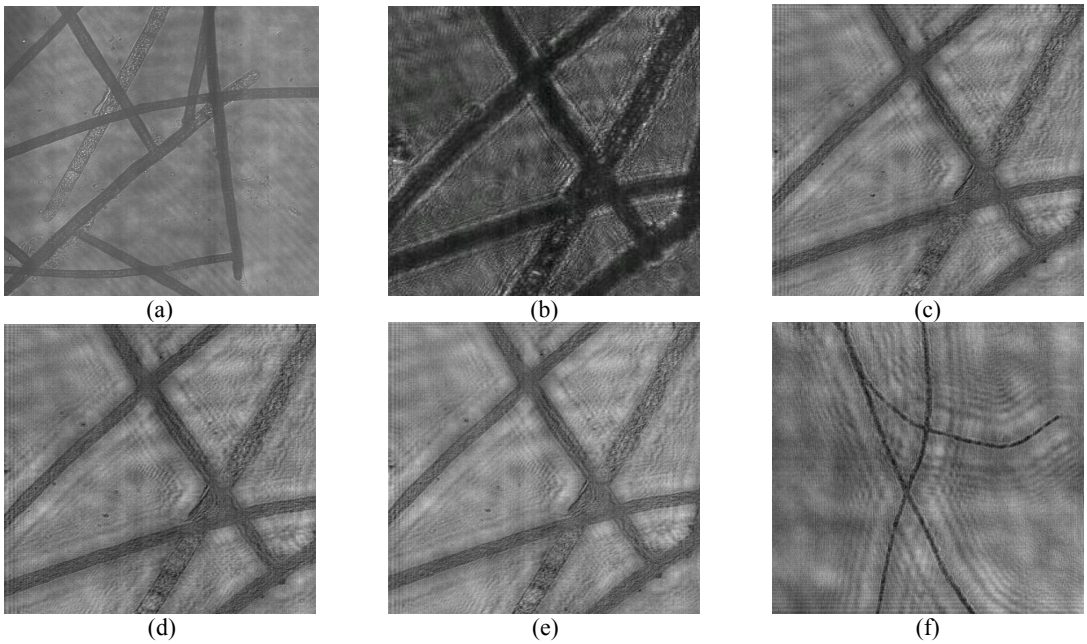

Fig. 3. Experimental results for biological samples (sphacelaria and tribonema aequale) by use of a 10× microscope objective, (a) sphacelaria's 2D image, (b) sphacelaria's digital hologram by SEOL digital holography, (c) and (d) sphacelaria's reconstructed images by use of SEOL digital holography with only single hologram recording at distance d =180 mm and 190 mm, respectively, (e) sphacelaria's reconstructed image at distance 180 mm using phase-shifting digital holography, (f) tribonema aequale's reconstructed image at distance d =180 mm using SEOL digital holography.

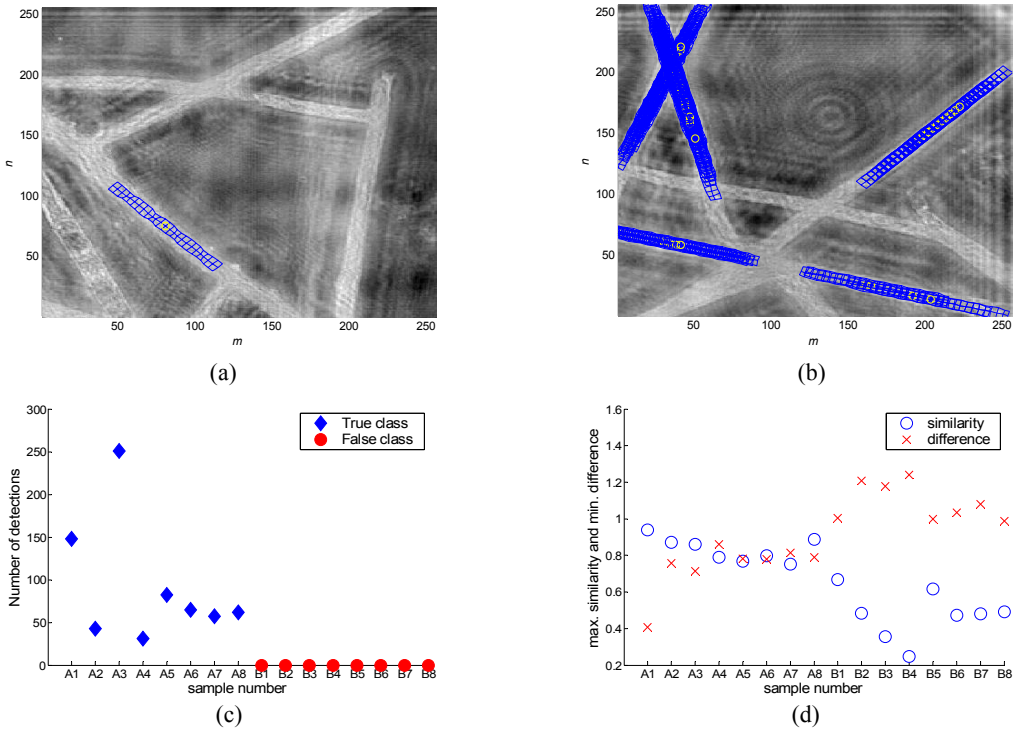

Fig. 4. (a) reference sample A_1 with the graph R, (b) graph matching result of one test sample A_8, (c) number of detections, (d) maximum similarity and minimum difference cost, (a) and (b) are presented by contrast reversal for better visualization.